Progress In Electromagnetics Research M, Vol. 19, 13–23, 2011

APPLICATION OF THE FRACTIONAL FOURIER TRANSFORM TO MOVING TRAIN IMAGING

L. Yu [1, 2, *] and Y. Zhang [2]

[1]Graduate University of the Chinese Academy of Sciences, Beijing 100039, China

[2]The Key Laboratory of Microwave Remote Sensing, Chinese Academy of Sciences, Beijing, China

Abstract—This paper introduces an imaging algorithm with application of fractional Fourier transform (FrFT) for ground moving train imaging by Ku-band ground-based radar. In view of the fact that the train speed is varying when acrossing the radar beam, the multiple Doppler parameters are estimated corresponding to different range positions, i.e., they are estimated from different sections of data in FrFT domain, then the train is imaged section by section, and finally these sectional images are combined to get the full image of the train. Because traditional parameter estimation method by two-dimensionally searching the peaks in FrFT domain is inefficient, we transfer the parameter searching problem into an one-dimensional optimization problem, which can be solved with high efficiency by using the golden section searching method.

1. INTRODUCTION

The fractional Fourier transform (FrFT), as a generalization of the classic Fourier transform (FT), has good energy concentration on linear frequency modulation (LFM) signals [1, 2]. It has been widely used in radar signal processing, such as beamforming [3], transient radar returns analysis [4], a modified chirp scaling algorithm for synthetic aperture radar (SAR) [5], inverse synthetic aperture radar (ISAR) imaging [6], and moving target detection [7].

Received 14 May 2011, Accepted 16 June 2011, Scheduled 23 June 2011

* Corresponding author: Lingjuan Yu (yljsmile@163.com).

Ground moving target imaged by ground-based radar is not studied widely as the ground moving target imaged by airborne or spaceborne SAR. In our experiment, moving train is imaged by a Ku-band ground-based radar. Although it seems like the ISAR imaging model should be adopted, it is not applicable in this case because the train is too long that even part of it can cover the all 3 dB beamwidth of the antenna due to small observation range. We know that the basic idea of ISAR imaging is based on the rotational model, which assumes that the targets should be totally exposed to the radar beam during the imaging time. We also know that the common condition should be met for both ISAR and SAR imaging is that there must exist relative motion between the target and the radar. We must point out that even we adopt the SAR imaging model, there are some differences, i.e., the influence of the clutter in real SAR case is usually unavoidable, but in our case, it plays almost no influence because their Doppler spectra are almost around zero frequency, which can be easily/directly removed in range-Doppler domain [8–10]. In [8], the detailed imaging process and the explanation of the electromagnetic scattering mechanism of the moving train were presented. In [9], Short Time Fourier transform (STFT) method was applied to analyzing the velocity variation of the train. It is well known that the variation of velocity will lead to the variation of Doppler parameters, and if constant Doppler parameters are used in imaging, the image results will be defocused definitely.

In this paper, the echo data are divided into several sections after range compression and range cell migration correction (RCMC), and the Doppler parameters corresponding to each section are estimated based on FrFT analysis and then used for imaging processing. At the end, the focused sections are combined together to form the final image. To speed up the process in FrFT, we transfer the parameter searching problem into an one-dimensional optimization (ODO) problem, which can be solved with high efficiency by using the golden section searching (GSS) method [11].

The rest of the paper is organized as follows. Section 2 briefly introduces the basic principle of FrFT and parameter estimation process in FrFT, discusses how to change the two-dimensional peak searching (TDPS) problem into an ODO problem, shows how the problem can be solved by the GSS method, and applies FrFT to SAR imaging. Section 3 introduces the imaging experiment, and applies FrFT to piecewise estimate the Doppler parameters aiming to obtain a well-focused image for the moving train. Finally, Section 4 concludes the paper.

2. BRIEF INTRODUCTION TO FRFT AND ITS APPLICATION IN SAR IMAGING

2.1. Definition

The FrFT of signal $s(t)$ is defined as [1],

$$S_p(u) = \int_{-\infty}^{\infty} K_p(t,u)s(t)dt, \quad 0 < |p| < 2 \tag{1}$$

where p is a real number and is called the order of the FrFT, $\alpha = p\pi/2$. The transform kernel $K_p(t,u)$ of the FrFT is given by,

$$K_p(t,u) = \begin{cases} \sqrt{\frac{1-j\cot\alpha}{2\pi}} \exp\left(j\frac{u^2+t^2}{2}\cot\alpha - jtu\csc\alpha\right) & \alpha \neq n\pi,\ (n=0,1,2\ldots) \\ \delta(t-u) & \alpha = 2n\pi \\ \delta(t+u) & \alpha = (2n+1)\pi \end{cases} \tag{2}$$

2.2. Parameter Estimation

As we know, the FrFT has the property of very good energy concentration on LFM signal (chirp). In the following, we shall introduce how the chirp's parameters can be estimated by using FrFT technique.

A chirp signal can be expressed as,

$$x(t) = s(t) + w(t) = A\exp\left(j\varphi_0 + j2\pi f_0 t + j\pi k_r t^2\right) + w(t),\ -\frac{\Delta t}{2} \le t \le \frac{\Delta t}{2} \tag{3}$$

where φ_0 denotes the initial phase, f_0 denotes the center frequency, k_r denotes the chirp rate, $w(t)$ denotes additive white Gaussian noise. The problem for estimating the center frequency and the chirp rate can be described by [12],

$$\{\alpha^*, u^*\} = \arg\max_{\alpha,u} |X(\alpha,u)|^2 \tag{4}$$

$$\begin{cases} \hat{k}_r = -\cot\alpha^* \\ \hat{f}_0 = u^*\csc\alpha^* \end{cases} \tag{5}$$

where $|X(\alpha,u)|$ represents the FrFT of $x(t)$. Equations (4) and (5) indicate that in order to get the center frequency f_0 and the chirp rate k_r, the best α^* and u^* are required first so as to get the energy of $|X(\alpha,u)|$ maximized.

Figure 1 depicts the parameter estimation process in FrFT domain according to the rotation of the time-frequency plane (t,f) [1]. If we can get the best estimation of rotation angle α^*, i.e., the best transform

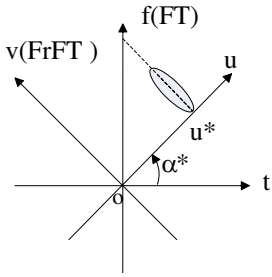

Figure 1. The parameter estimation in FrFT domain.

order p^* of FrFT because $\alpha^* = p^*\pi/2$, and its location u^* in u domain, then f_0 and k_r will be obtained according to (5). Fig. 1 also shows that the FT just corresponds to the rotation angle $\alpha = \pi/2$, which indicates that the FrFT is the generalized form of the classic FT.

2.3. Determination of Transform Order

The regular method for determing the transform order of FrFT is by carrying out a TDPS process, this is very time-consuming. However, the TDPS problem in Equation (4) can be transformed into the ODO problem, which can be solved by two steps. The first step is to let α be fixed, and to calculate the $X_\alpha(u)$ by fast Fourier transform (FFT), and then $\max\limits_u |X_\alpha(u)|^2$ can be obtained by sorting with fast algorithm [13]. The second step is to solve the maximization problem of $\max\limits_\alpha(\max\limits_u |X_\alpha(u)|^2)$. If we define the objective function $f(\alpha) = -(\max\limits_u |X_\alpha(u)|^2)$, then the ODO problem can be expressed as,

$$\min_\alpha f(\alpha) \tag{6}$$

There are many methods for solving the ODO problem, such as, the GSS method, Fibonacci method, and Newton method. Because the GSS method is very simple, efficient and stable [11], we will use it in Section 3.2.

2.4. Azimuthal Parameters Estimation Based on FrFT for SAR Imaging

In the conducted experiment [8], the big squint angle brings much difficult for RCMC especially for wide beam case. However, we still can perform RCMC by selecting appropriate viewing angle and the train speed so as to make the resulted scatterers corresponding to different range bins aligned as straight as possible. Due to the wide beam of

antenna, the range cell migration cannot be very accurately corrected. In fact, the azimuthal signal after RCMC can be well treated as a chirp signal, so FrFT can be applied to estimating its parameters used for azimuthal matched filtering.

In the range-Doppler imaging algorithm for SAR, the matched filter in azimuth can be constructed by [14],

$$s_a(t_m) = A_a(t_m) \exp\left(j2\pi f_{dc} t_m + j\pi K_a t_m^2\right) \tag{7}$$

where t_m, $A_a(t_m)$ are respectively the slow time and amplitude in azimuth, and the Doppler centroid frequency f_{dc} and Doppler rate K_a can be approximated by [14],

$$\begin{cases} f_{dc} \approx \frac{2v \sin\theta_0}{\lambda} \\ K_a \approx -\frac{2v^2 \cos^2\theta_0}{\lambda R_0} \end{cases} \tag{8}$$

where λ, v, θ_0 and R_0 are the wavelength, speed, view angle and squint range from radar to the center of targets, respectively.

In real data collection, parameters v, θ_0 and R_0 may be slightly changed during the imaging time, but if they are treated as constants and used for calculating Doppler parameters through (8), then we can not get a well-focused image. One efficient way to solve the problem is to divide the data after RCMC into several sections, so the Doppler parameters in each section can be treated as constants, which can be obtained in FrFT domain. In the following, we shall process the experimental data to show the effect of the algorithm.

3. EXPERIMENTAL RESULTS

3.1. Experiment Description

The experimental radar system includes three standard-gain horn antennas (one used for transmitting, and two used for receiving), one frequency synthesizer, one two-channel receiver, one transmitter, and data recording devices [8]. The typical technical parameters are listed in Table 1. The train's optical picture and the radar imaging geometry are shown in Fig. 2.

Table 1. Typical radar system parameters.

Central frequency	13.58 GHz
Antenna gain	25 dB
3 dB beamwidth	10°
Bandwidth	100 MHz
Pulse Width	20 μs

(a) Optical picture of the train

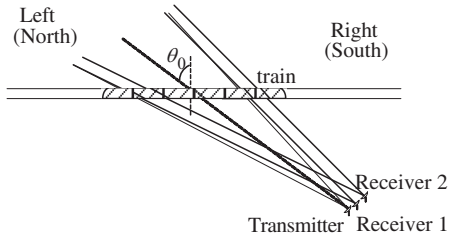

(b) Radar imaging geometry

Figure 2. The train's optical picture and the radar imaging geometry.

3.2. Imaging Processing and Results

The imaging processing for the moving train mainly includes the correction of system amplitude and phase errors, range compression, motion compensation and clutter suppression [9]. In this section, we just briefly introduce the range migration correction, but the detailed azimuth compression based on FrFT with two different searching methods for parameters estimation.

Let's denote the echo signal after matched-filtering compression in range direction $s(t, t_m)$, where t and t_m respectively denote the fast time and the slow time. The range migration correction can be done after correction of system error as [8, 9]:

$$s_{rc}(t, t_m) = IFFT_f \left\{ FFT_t[s_{pc}(t, t_m)] \cdot \exp\left(-j4\pi \frac{v t_m \sin\theta_0}{c} f \right) \right\} \quad (9)$$

where $s_{pc}(t, t_m)$ denotes the signal after preliminary correction of system error, $s_{rc}(t, t_m)$ denotes the time-domain signal after range migration correction. v and θ_0 are the velocity of the train and the view angle of radar system, respectively, which are estimated from echo data as illustrated by the formulae. The two-dimensional data after range migration correction is shown in Fig. 3. Just as explained above because only linear range migration is considered and the parameters v and θ_0 are estimated from echo data, there are still some errors.

The final image of the moving train can be obtained after azimuth compression [8, 9]:

$$s_{im} = IFFT \left\{ FFT_{t_m} \left[s_{rc}(t, t_m) \right] \cdot FFT_{t_m} \left[s_a^*(t_m) \right] \right\} \quad (10)$$

where $s_a(t_m)$ is the matched filter in azimuth. It can be expressed as,

$$s_a(t_m) = \exp\left(j2\pi f_{dc} t_m + j\pi K_a t_m^2 \right) \quad (11)$$

where f_{dc} and K_a are Doppler centroid frequency and Doppler rate, respectively.

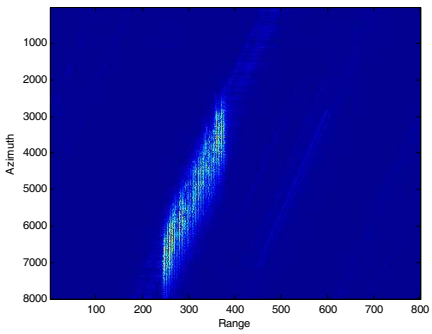

Figure 3. The 2D data in time domain after range compression and RCMC.

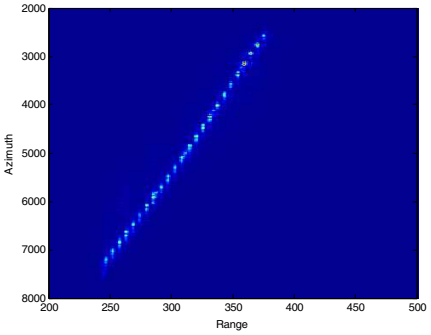

Figure 4. The amplitude radar image of the moving train.

Equation (11) with the amplitude term omitted is almost as same as Equation (7), and its parameters can be calculated by (8) with constant v, θ_0 used. Fig. 4 shows the final amplitude image. It is obvious that there are some scatterers not well-focused. The image entropy of 9.4849 is listed in Table 3.

Since the train moves at varying speed when acrossing the radar beam, this will lead to varying f_{dc} and K_a. Because at an instant time period only some part of the train is in the radar beam, different part of the train may experience different velocities. As illustrated in Section 2.4, FrFT can be used to piecewise estimate the Doppler parameters in (11), assuming the variation of train speed in each small section can be ignored.

Now, we partition the echo data $s_{rc}(t, t_m)$ obtained after range migration correction into three sections (of course, the more sections, the finer the Doppler parameters estimated) according to range bins. The first section ranges from bin 1 to bin 286, the second section ranges from bin 287 to bin 327, and the third section ranges from bin 328 to bin 800. For each section, f_{dc} and K_a are estimated in FrFT domain. In the following, two methods will be applied to estimating the best transform order of FrFT, thus the f_{dc} and K_a parameters.

First, the two-level searching method, as one of the usually used two-dimensional searching methods is adopted. For the first range section, the initial searching area of α is $[0, 2\pi]$, and the step length of the first level coarse searching is 0.01, and step length of the second level refined searching is 0.0001. For the second range section, the initial value of searching is set to be the final transform order of the first section because of the correlation between the two adjacent sections, so only the second level refined searching is implemented. In the same

way, for the third section, the initial value of searching is the final transform order of the second section, and only the second level refined searching is implemented. All of the estimated parameters and the corresponding consumed time are listed in Table 2.

Figures 5, 6 and 7 present the obtained SAR images using the Doppler parameters estimated from the first section, the second section and the third section, respectively. Just as expected that when using the Doppler parameters estimated from the first section, only the corresponding first section of the train is well focused, when using the Doppler parameters estimated from the second section, only the corresponding second section of the train is well focused, and when using the Doppler parameters estimated from the third section, only the corresponding third section of the train is well focused.

It is obvious that if we pick up the first section from Fig. 5, the second section from Fig. 6, and the third section from Fig. 7, to form a new SAR image, then we can get the final image with all of the sections well focused. Fig. 8 shows the final imaging result.

Second, the GSS method introduced in Section 2 is adopted. The initial searching area of α is also set to $[0, 2\pi]$. Repeat the above imaging steps with different Doppler parameters estimated from the

Table 2. Doppler parameters and computing time.

	The first section			The second section			The third section		
	f_{dc} (Hz)	Ka (Hz/s)	Computing Time (s)	f_{dc} (Hz)	Ka (Hz/s)	Computing time (s)	f_{dc} (Hz)	Ka (Hz/s)	Computing time (s)
Two-level searching method	–195.4222	–30.8495	7.7343	–219.8546	–24.9329	5.4899	–247.6409	–19.7419	5.4943
Golden section searching method	–195.4244	–30.8612	0.4014	–219.8554	–24.9376	0.3651	–247.6416	–19.7462	0.3730

Table 3. Image entropy in different cases.

	Constant Doppler parameters	Doppler parameters estimation based on FrFT	
		The Two-level searching method	The Golden section searching method
Image entropy	9.4849	8.8170	8.8168

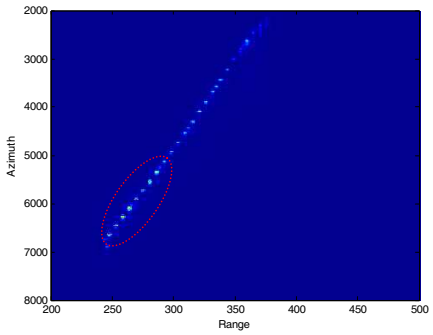

Figure 5. The obtained image by using the Doppler parameters estimated from the first section.

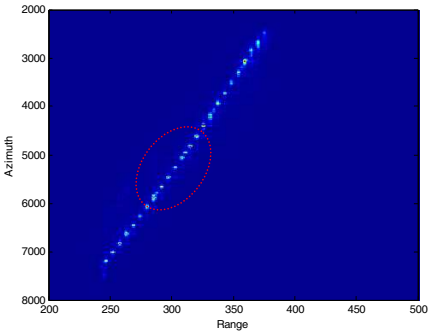

Figure 6. The obtained image by using the Doppler parameters estimated from the second section.

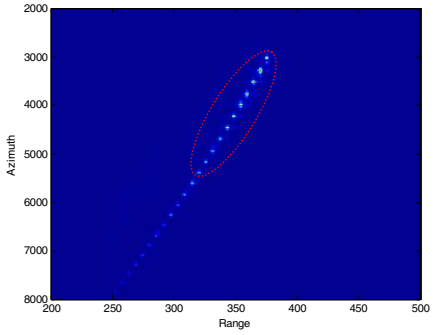

Figure 7. The obtained image by using the Doppler parameters estimated from the third section.

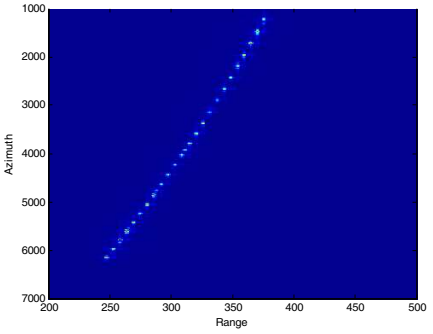

Figure 8. The final image obtained by using the two-level searching method.

data in different sections, and combine the three well-focused sections into a final image shown in Fig. 9. It is better than Fig. 4, and its entropy is listed in Table 3. All the estimated parameters and computing time are also listed in Table 2. Once again as we expected that the obtained image is as good as that obtained by the first approach but with much less time used.

As the optical picture in Fig. 1(a) shows that the train has 6 compartments, and each compartment has 4 same doors and 3 same windows. The reason why the radar image of the train is slightly curved and is not a straight line as we expect is because the train is on a slightly curved bridge. From Fig. 4 to Fig. 9, the radar images include the major electromagnetic scattering information of the moving train. For detailed scattering analysis please refer to [8].

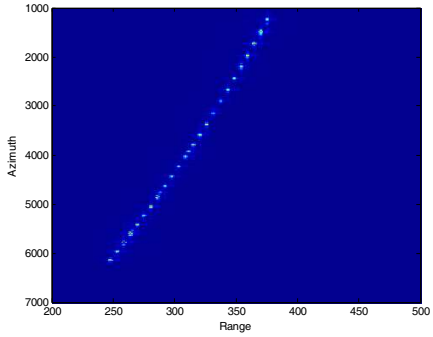

Figure 9. The final image obtained by using the golden section searching method.

4. CONCLUSION

In this paper, the FrFT is applied to the Ku-band ground-based radar imaging of ground moving train. The imaging results show that the method with sectional Doppler parameters estimation based on FrFT is very suited for moving target imaging with varying velocities. In order to reduce the computing time in parameter estimation in FrFT domain, the two-dimensional parameter searching problem is transferred into an ODO problem. The experimental results show that by using the GSS method, the computing time can be significantly reduced compared with that of the two-dimensional parameter searching method with almost the same quality achieved.

REFERENCES

1. Almeida, L. B., "The fractional Fourier transform and time-frequency representations," *IEEE Transactions on Signal Processing*, Vol. 42, No. 11, 3084–3091, 1994.
2. Haldum Ozaktas, M., et al., "Convolution, filtering, and multiplexing in fractional Fourier domains and their relation to chirp and wavelet transforms," *J. Opt. Soc. Am. A*, Vol. 11, No. 2, 547–559, 1994.
3. Yetik, I. S. and A. Nehorai, "Beamforming using the fractional Fourier transform," *IEEE Trans. Signal Processing*, Vol. 51, No. 6, 1663–1668, 2003.
4. Jang, S., W. Choi, T. K. Sarkar, et al., "Exploiting early time response using the fractional Fourier transform for

analyzing transient radar returns," *IEEE Trans. Antennas and Propagationm*, Vol. 52, No. 11, 3109–3121, 2004.

5. Amein, A. S. and J. J. Soraghan, "A new chirp scaling algorithm based on the fractional Fourier transform," *IEEE Signal Process. Lett.*, Vol. 12, No. 10, 805–807, 2005.
6. Borden, B., "The fractional Fourier transform and ISAR imaging," *Inv. Probl. Lett.*, Vol. 16, No. 2, 5–8, 2000.
7. Sun, H.-B., G.-S. Liu, H. Gu, et al., "Application of the fractional Fourier transform to moving target detection in airborne SAR," *IEEE Transactions on Aerospace and Electronic Systems*, Vol. 38, No. 4, 1416–1424, 2002.
8. Zhang, Y., X. Zhang, W. Zhai, et al., "Radar imaging and electromagnetic scattering analysis for ground moving target by ground-based stationary radar," *Asia Pacific Microwave Conference*, 2224–2227, 2009.
9. Zhang, Y. H., Y. Deng, W. S. Zhai, X. K. Zhang, and J. S. Jiang, "Time-frequency processing and analysis of radar imaging experiment data for a moving train," *The 7th Iasted International Conference on Antennas, Radar and Wave Propagation*, Cambridge, Massachusetts, USA, Nov. 1–3, 2010.
10. Zhang, Y., X. Zhang, W. Zhai, et al., "Moving train imaging by ground-based Ka-band radar," *The 6th Loughborough Antennas & Propagation Conference*, 413–416, Loughborough, 2009.
11. Xue, L., *Optimization Techniques in Engineering*, Tianjing University Press, Tianjing, 1989 (in Chinese).
12. Lin, Q., T. Ran, and S. Zhou, "Detection and parameter estimation of multi-component LFM signal based on the fractional Fourier transform," *Science in China: Series F Information Science*, Vol. 47, No. 2, 184–198, 2004.
13. Ozaktas, H. M., O. Arikan, M. A. Kutay, et al., "Digital computation of the fractional Fourier tansform," *IEEE Transactions on Signal Processing*, Vol. 44, No. 9, 2141–2150, 1996.
14. Cumming, I. G. and F. H. Wong, *Digital Processing of Synthetic Aperture Radar Data: Algorithms and Implementation*, Artech House Publishers, 2005.